Powder Technology 431 (2024) 119096

Contents lists available at ScienceDirect

Powder Technology

journal homepage: www.journals.elsevier.com/powder-technology

Bubble self-organization in pulsed annular gas-solid fluidized beds

Kaiqiao Wu [a,1], Shuxian Jiang [a,1], Victor Francia [b], Marc-Olivier Coppens [a,*]

[a] EPSRC "Frontier Engineering" Centre for Nature-Inspired Engineering, Department of Chemical Engineering, University College London, London, WC1E 6BT, United Kingdom

[b] Institute of Mechanical, Process and Energy Engineering, Heriot-Watt University, Edinburgh, EH14 4AS, United Kingdom

HIGHLIGHTS

- Structured flow is reproduced in annular pulsed fluidized beds.
- Difference of bubble properties between rectangular and annular beds is researched.
- Effect of curved and lateral walls on pattern regularity is explored.
- A correlation is drawn to estimate the operating conditions for structured flow.
- CFD-DEM simulations are used to study solid motion in annular beds.

GRAPHICAL ABSTRACT

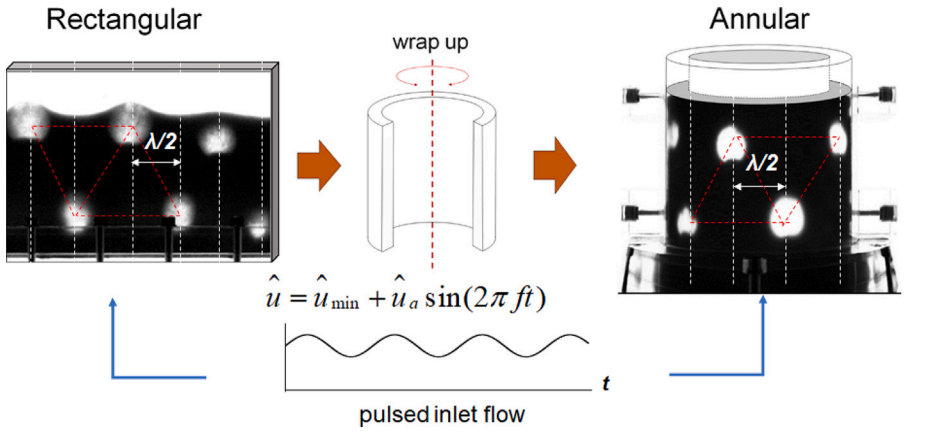

ARTICLE INFO

Keywords:
Pattern formation
Scale-up
CFD-DEM
Bubble control
Modularization
Particle processing

ABSTRACT

Pulsating the gas flow in rectangular, quasi-2D fluidized beds can turn the chaotic bubble flow into a regular bubble pattern. Bubbles form a rising triangular lattice, leading to a scalable flow structure with controllable properties, such as narrow bubble size distribution, distance between bubbles, and residence time. This overcomes challenges encountered in conventional units, like flow maldistribution and non-uniform contact. In this work, we reproduced a similar, dynamically structured flow in a cylindrical annular geometry. Regular bubble patterns emerge along the circumference of the cylinder. The absence of lateral walls and strongly curved boundaries could cause instabilities. This study presents an operating window for creating spatiotemporally structured flows and compares the flow properties in quasi-2D rectangular and annular systems, quantifying the impact of curvature and, effectively, lateral walls on flow behavior. These insights offer new opportunities for modularization of fluidized bed operations.

1. Introduction

Gas-solid bubbling fluidized beds (BFBs) are widely employed as reactors in chemical, oil, biomass and waste conversion, pharmaceutical, biotechnological and functional materials industries, owing to their efficient gas-solid contact and good mass and heat transport rates [1]. Their overall performance relies significantly on the macroscopic bubble flow. In a BFB, bubble motion is irregular, and solids circulate in complex, scale-dependent patterns [2,3]. For these chaotic hydrodynamics, effective operation and proper scale-up of a BFB remain largely empirical exercises, because they depend on many parameters which

* Corresponding author.
E-mail address: m.coppens@ucl.ac.uk (M.-O. Coppens).
[1] These authors contributed equally.

https://doi.org/10.1016/j.powtec.2023.119096
Received 18 July 2023; Received in revised form 30 September 2023; Accepted 24 October 2023
Available online 27 October 2023

Nomenclature

Symbols

$\hat{u}$	Normalized superficial gas velocity [–]
$\hat{u}_{\min}$	Normalized offset of the oscillatory flow [–]
$\hat{u}_a$	Normalized amplitude of the oscillatory flow [–]
A_1, A_2	Measured and calibrated area of the bubble [cm^2]
D	External diameter of the annular bed [cm]
D_b	Bubble diameter [cm]
d_p	Particle diameter [cm]
f	Oscillatory flow frequency [Hz]
f_{b,ϕ_0}	Bubble phase probability density [–]
H	Bed height [cm]
H_b	Initial bed height [cm]
L_1, L_2	Measured and calibrated bubble length in the azimuthal direction [cm]
M	Magnification factor [–]
R	External radius of the annular bed [cm]
t	Flow time [s]
u	Superficial gas velocity [cm/s]
u_{mf}	Minimum fluidization velocity [cm/s]
V_p	Particle velocity [cm/s]
$V_{s,x}, V_{s,y}$	Solids lateral velocity and axial velocity [cm/s]
W	Bed length [cm]
x, y	Cartesian coordinates with x lateral and y vertical [cm]
X_1, X_2	Measured and calibrated lateral positions of bubble center [cm]
Z	Bed thickness [cm]

Greek Symbols

δ_b, δ_λ	Span of bubble diameter and wavelength [–]
Λ	Pattern intensity [–]
λ	Pattern wavelength [cm]
ϕ	Volume fraction of solid phase [–]
φ	Phase angle [–]

may not change concordantly with each other and may drastically deteriorate the performance [4].

Over the past decades, continuous efforts have been made to facilitate scaling up bubbling fluidized bed reactors. The traditional approach focuses on identifying scaling laws with relevant dimensionless parameters and ensuring hydrodynamic similarity between fluidized beds of different scales [5,6]. One limitation to this approach for industrial applications is the lack of degrees of freedom. Fundamental operational design changes could overcome the disadvantages associated with chaotic dynamics, by creating "structured" fluidized beds by introducing additional degrees of freedom to the system [7]. A structured bed implies that it is more predictable, homogeneous and controllable than a traditional fluidized bed. There are various methods to manipulate the fluidization behavior, such as applying internals [8], a magnetic field [9], acoustic excitation [10], vibration [11,12], and flow pulsation [13,14].

Our previous works demonstrate a way to structure gas-solid BFBs utilizing dynamic self-organization [3,15–18]. Complex spatially and temporally self-organized patterns can be generated by imposing periodic perturbations to dissipative, granular systems. There are many examples in nature, such as the ordered ripples on sandy beaches and dunes (Fig. 1a). This pattern formation suggests a solution to stabilize inherently chaotic granular systems. Drawing inspiration from nature, one can recreate various such patterns at the lab-scale, such as surface patterns (e.g., stripes, squares, hexagons) in shallow granular layers obtained via periodic mechanical vibration or oscillating flows (Fig. 1b) [18,19]. Pulsation and vibration are two common tools to improve the fluidization quality [11,20], and they are also currently known as effective ways to trigger the formation of periodic patterns in granular systems. Pulsed fluidization was found to suppress chaotic behavior in a BFB [16,21]. Strikingly different from the chaotic hydrodynamics of a traditional BFB, the introduction of oscillatory flow creates fully regular and predictable flow structures, in which bubbles self-organize dynamically along rising, periodic triangular lattices with a controlled pattern wavelength, and alternate their positions every period [22], see Fig. 1c.

Over the past few years, we have applied this approach to create fully structured macroscopic flows in relatively deep, rectangular quasi-2D BFBs. Bubble dynamics are found to be directly associated with the pulsed flow properties, leading to a relatively broad operating regime where critical bubble properties such as size and separation can be externally controlled [23]. To understand its formation and stability, the structured flow in a quasi-2D pulsed fluidized bed was first successfully simulated by using a three-dimensional coupled Discrete Element Method for the particles and Computational Fluid Dynamics for the gas phase (CFD-DEM) [15]. Recently, Guo et al. reported a similar periodic triangular structuring of bubbles in a quasi-2D vibrated fluidized bed, and a constitutive relationship for frictional solids stress was proposed in their work, which was validated to predict the structured bubble flow by bridging the viscous and the plastic regime [24].

In this way, the overall hydrodynamics can be manipulated in a controllable manner. Nevertheless, to explore the potential of structured fluidization in engineering applications, there are still some outstanding issues. Firstly, structured flow is limited by bed height: as bed height increases, the degree of order in the bubble dynamics and the operating regime were found to decrease [23]. Secondly, all existing research is based on quasi-2D, rectangular beds. It is not easy to implement structured fluidization in current 3D systems; many industrial units are either cylindrical or have internals. The effect of the curvature of the wall or the cylindrical geometry on the stability of this structured phenomenon remains unclear. In order to overcome these limitations, Guo et al. [25] proposed a layered configuration of fluidized beds, which separates different layers by multiple stages of gas distributors. Their CFD-DEM simulation results on a vibrated quasi-2D fluidized bed demonstrate that the bubble flow can reach the same stability and regularity in two adjacent layers. However, this staged configuration also leads to an increased total pressure drop and energy cost, and further experiments are necessary to prove the feasibility of this layered structured fluidized bed.

Recently, we have proposed a different way to recreate a similar structured flow in a cylindrical set-up, see Fig. 1d, extending it from a flat to an annular configuration. Note that it is far from obvious that this would also lead to a regular bubble pattern. In addition, the influence of wall effects on the bubble dynamics is believed to be important in a thin fluidized bed system [26,27]. A recent experimental investigation on a quasi-2D pulsed fluidized bed has revealed that the flow pattern is influenced by the interaction between particles and the lateral walls. The solid dispersion in this system can be regarded as a sub-diffusive process [28]. When extending the system from a quasi-2D flat configuration to an annular one, the walls are no longer planar, but curved surfaces. Therefore, the effects of the absence of lateral walls and strongly curved boundaries need to be carefully examined.

This work aims at extending the structured flow from a quasi-2D flat bed to an annular bed as a way to explore the robustness of the pattern in different configurations of interest to practical applications in 3D modular fluidized bed designs. The reproducibility, bubble and solid flow properties were investigated by varying pulsation parameters in experiments and CFD-DEM simulations. To quantify the impact of curved walls and the absence of lateral walls on the flow behavior, the flow properties in an annular cylindrical bed were compared with previous research in a quasi-2D flat bed.

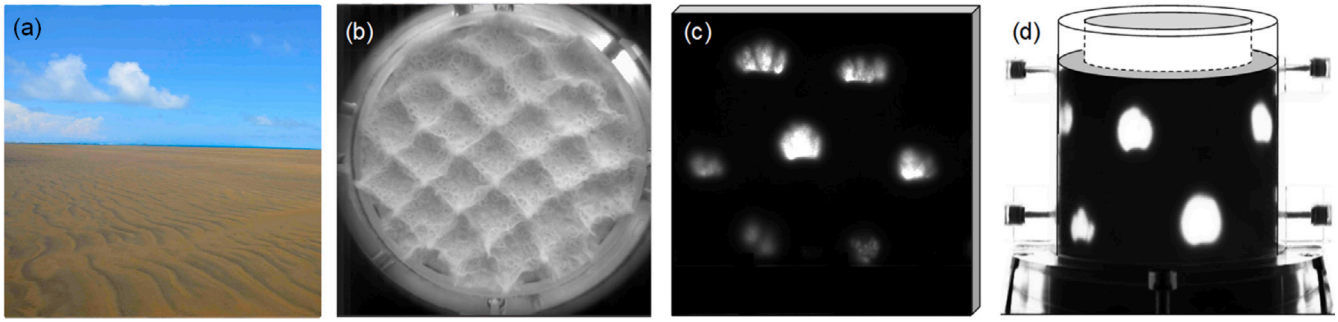

Fig. 1. (a) Natural granular patterns (photograph by M.-O. Coppens), and (b)–(d) formation of structured patterns under oscillatory flows. Pattern formation in periodically perturbed natural dissipative systems has inspired the initiation of (b) surface waves in pulsed shallow layers, (c) structured flows of bubbles in a pulsed quasi-2D, rectangular bed, and (d) an annular, cylindrical bed.

2. Experimental methodology

2.1. Experimental setup

The annular cylindrical fluidized bed setup is schematically presented in Fig. 2. The bed was fabricated from Plexiglass. It has a thickness Z of 1 cm and an external diameter D of 14 cm, so that the circumference of the annular bed is approximately the same as the width of the quasi-2D rectangular bed used in previous studies (45 cm) [15,17]. Uniform distribution of the gas velocity at the inlet boundary was achieved through a 3 mm thick, porous bronze disc (Grade 07, BK 10.30.07, Sintertech) and complex fillers in the plenum chamber. Fluctuations of the flow passing through the solenoid valve affect all flows, which can be a source of error in this configuration. Therefore, a reservoir tank was added before the valves, which helps to decrease the fluctuations and improve measurement accuracy, as well as eliminate the effect of back-flow induced by the solenoid valve in the upstream flow. Spherical glass beads were tested as fluidized particles and were sieved prior to the start of the experiments to obtain a controlled particle size distribution, with a particle diameter d_p = 225 μm ∼ 250 μm, which can be classified as Geldart B particles.

Particles in the experiments were fluidized using dry air at atmospheric pressure. The oscillatory gas flow was generated by a gas supply system consisting of valves, flow meters, filters, a gas reservoir, and a MKS 154B type proportional solenoid valve, which was controlled by a LabVIEW panel to create sinusoidal waves. Two flow meters were used in this experiment and were calibrated with a FLUICAL portable mass flow calibrator. The minimum fluidization velocity u_{mf} of this system is 4.0 cm s^{-1}. A pulsed superficial gas velocity u is normalized by u_{mf}, and the normalized inlet sinusoidal pulsed flow velocity $\hat{u} = u/u_{mf}$ is given as below:

$$\hat{u} = \hat{u}_{min} + \hat{u}_a[1 + \sin(2\pi f t)] \quad (1)$$

where $\hat{u}_a$ and $\hat{u}_{min}$ are the normalized amplitude and minimum velocity of the applied oscillatory flow, respectively, and f denotes the oscillating flow frequency. Experiments were conducted for continuous and pulsed flow with different conditions, as shown in Table 1.

The setup was illuminated using a LED panel and LED spotlights. The LED light crosses the Plexiglass shell and creates a sharp contrast between the bubble and emulsion phase. To do so, a flexible LED strip was distributed uniformly along the surface of a cylinder smaller than the inner diameter of the annular fluidized bed, and this cylinder was placed in the centre of the annular bed during the experiment to allow illumination in the radial direction. A square 595 mm × 595 mm LED backlit panel (ROBUS, 40 W) was vertically placed behind the fluidized bed, providing background illumination of the bubbles. The bubble flow was recorded at 100 frames per second and a resolution of 1696 × 1696 pixels, using a Basler digital camera (acA1920-150 μm) equipped with a wide-angle lens (MachineVision M1224-MPW2).

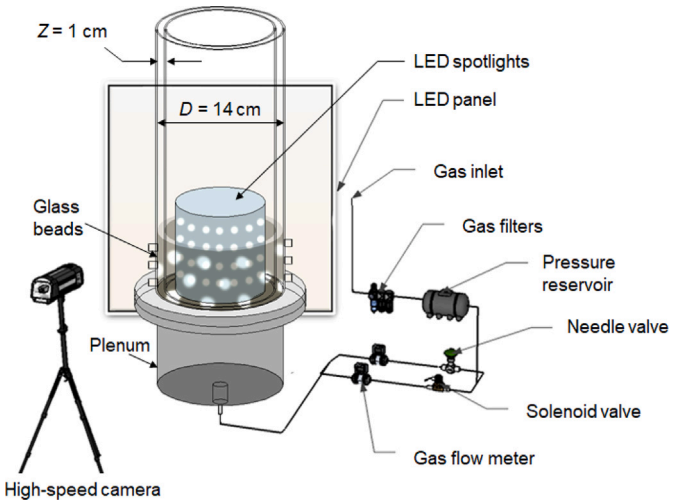

Fig. 2. Schematic of the annular, cylindrical fluidized bed setup with pulsed gas flow.

Table 1
Experimental conditions investigated.

Symbol	Parameter	Range
f	Frequency (Hz)	3–10
$\hat{u}_a$	Normalized pulse amplitude	1.25–2.75
$\hat{u}_{min}$	Normalized pulse minimum velocity	0.5–1.25

2.2. Numerical model

In this work, the Euler–Lagrange model was adopted to simulate the hydrodynamics of the gas-solid flow in an annular cylindrical bed; the model settings were consistent with our previous work on a quasi-2D rectangular bed [17]. Simulations were performed utilizing the open-source code CFDEM®coupling v3.8.0 [29], which employs a four-way coupled solver. Particles were assumed to be spherical and of the same size, and a Hertzian interaction model was applied to calculate normal and tangential forces acting on the particles. Gas and particle motions were linked using Gidaspow's drag law [30], which combines the empirical correlations of Wen and Yu [31] and Ergun [32] for dilute and dense regions of the bed, respectively. The simulated domain is shown in Fig. 3.

In order to reduce the computational cost and facilitate the comparison with our previous simulations of the rectangular configuration, the domain was reduced to a quarter annular bed with a bed thickness Z = 0.2 cm. As shown in Fig. 3, a structured mesh was employed, and the mesh size of the fluid cells was set to be 0.2 cm. The model has been validated in our previous study [15] and it was shown that this mesh

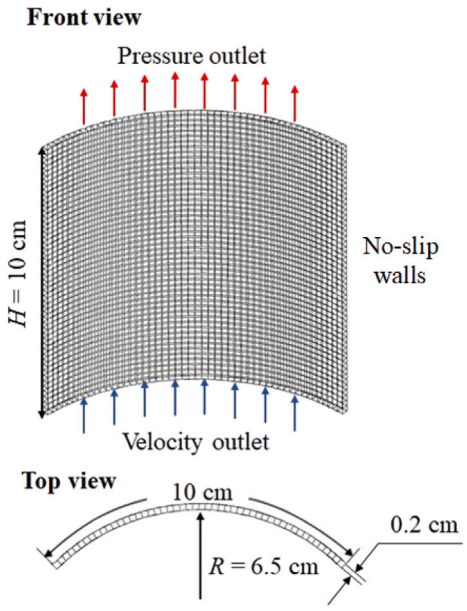

Fig. 3. The computational domain of the simulated annular fluidized bed and the applied boundary conditions. A no-slip wall condition is applied to all the side boundaries.

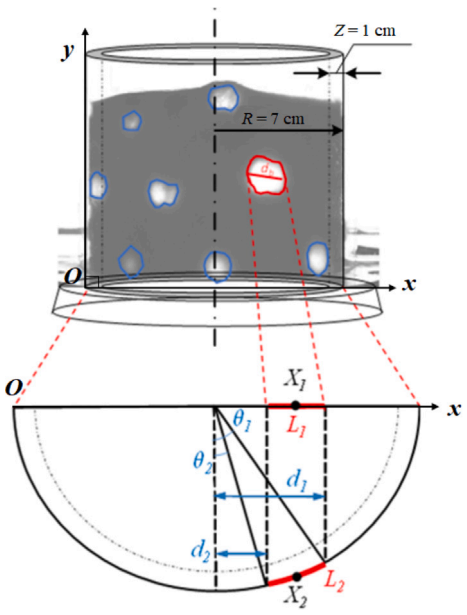

Fig. 4. Calibration of bubble position and size in the annular bed.

size is able to achieve adequate flow field resolution and maintain grid-independent simulation results. For the inlet boundary, the gas velocity was set to $\hat{u} = 0.45+1.9[1+\sin(2\pi 5t)]$. The top surface was set as pressure outlet, while the surrounding surfaces in the domain were specified as non-slip walls.

2.3. Bubble identification

To quantitatively evaluate the bubble flow, ImageJ software (NIH, Bethesda, MD) and MATLAB (The MathWorks Inc., Natick, MA, USA) were used to post-process the images recorded by camera. In CFD-DEM simulations, a bubble is defined as a closed region where the solid volume fraction ϕ is lower than a threshold value $\phi_b = 0.2$. As shown in Fig. 4, taking into account the curvature of the annular fluidized bed, it is necessary to perform a transformation that unwraps the flow pattern into a flat image. A magnification factor M can be determined by the measured bubble length L_1 and position. The bubbles were assumed to be rounded in shape and the formula for this calibration is given below.

$$\begin{cases} \theta_1 = \sin^{-1}(d_1/R); \theta_2 = \sin^{-1}(d_2/R) \\ L_2 = R(\theta_1 - \theta_2); L_1 = d_1 - d_2 \\ M = L_2/L_1 \end{cases} \tag{2}$$

where L_2 refers to the calibrated bubble length in the azimuthal direction, and R is the external radius of the annular bed. The distances of the bubble from the cylindrical axis are denoted by d_1 and d_2, corresponding to the maximum and minimum values, respectively. The angular positions of these two points are given by θ_1 and θ_2. The image is not stretched in the axial direction and the vertical dimension remains unchanged. Therefore, the calibrated bubble area A_1 and the lateral position of bubble center X_2 can be calculated as:

$$\begin{cases} A_2 = A_1 M \\ X_2 = R\{\pi/2 + \sin^{-1}[(X_1 - R)/R]\} \end{cases} \tag{3}$$

where A_1 is the measured bubble area, and X_1 is the lateral position of the measured bubble center. The actual bubble size can be calibrated by determining the corresponding arc length. After calibration, the equivalent bubble diameter D_b is calculated as the diameter of the perfect circle with the same area A_2, $D_b = \sqrt{4A_2/\pi}$. The estimation can cause large deviations only if the bubbles are extremely irregular in shape. Another characteristic parameter of the bubble pattern, the wavelength λ is defined as the median of the calibrated distances between centroids of neighboring bubbles.

The phase angle φ is applied to describe reproductions of the evolution of flow structures in a pulse. φ is expressed as $\varphi = 2\pi(t-t_0)/T$, where $T = 1/f$ refers to one pulse period and t_0 stands for any integer multiple of T. To evaluate the self-organization process and its reproducibility, pattern intensity Λ is used. A model based pattern recognition algorithm is employed to compute Λ; more details can be found in [23]. Briefly, Λ corresponds to the level of cross-correlation among bubbles: $\Lambda = 1$ indicates bubbles perfectly aligned in a spatial–temporal pattern, while $\Lambda = 0$ denotes a statistically random placement. To also characterize the broadness of the distribution, a dimensionless index span δ is used and calculated by Eq. (4),

$$\delta_x = \frac{D_{90} - D_{10}}{D_{50}} \tag{4}$$

where D_{10}, D_{50}, and D_{90} are the values in distributions greater than 10%, 50%, and 90% of the sample, respectively. The subscript x is d for bubble size and λ for bubble wavelength, respectively. The wider the distribution, the larger the span value.

3. Results and discussion

This section presents a comparative analysis of bubble flows in both quasi-2D rectangular and annular cylindrical geometries. Key properties such as flow patterns, bubble size control, bubble spatial arrangement, and homogeneity are experimentally assessed for their reproducibility across different configurations. In addition, simulations of both bed types are carried out in smaller domains ($W \times H \times Z$ = 10 × 10 × 0.2 cm, initial bed height H_b = 4.5 cm) to facilitate a direct comparison, and provide insights into the translatability of flow properties.

3.1. Recreating flow patterns in the annular cylindrical configuration

By applying the same pulsation conditions leading to structured flows in the rectangular system, a correspondingly robust, structured

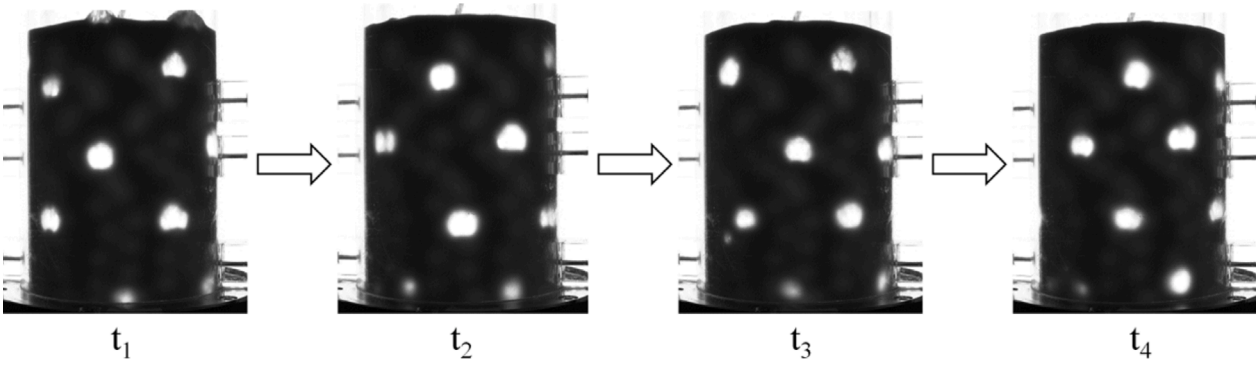

Fig. 5. Dynamically structured flow of bubbles in an annular bed. Representative frames sampled from consecutive gas pulsation periods, at t_1, $t_2 = t_1 + 1/f$, $t_3 = t_1 + 2/f$, $t_4 = t_1 + 3/f$. Dark, continuous phase represents emulsion phase, whereas bright, dispersed phase represents bubble phase. $d_p = 238$ μm, $H_b = 20$ cm, $\hat{u} = 0.5 + 1.75[1 + \sin(2\pi 5t)]$.

flow pattern emerges in the annular configuration. Two critical differences characterize the annular system: it has no lateral walls and it introduces curved boundaries. Despite these geometric variations, the bubble flow appears as a periodically structured flow, exhibiting no lateral edges of the pattern, as depicted in Fig. 5. The modification to the geometry imposes only minimal impact on the manifestation of the structured flows, highlighting the adaptable nature of the structured flow across various configurations.

In the absence of the stabilization effect provided by the lateral walls, the flow within the annular geometry can be conceptualized as adhering to a periodic boundary condition, for which the left and right ends of the flow domain are connected. It is noteworthy that the bubble flows exhibit adaptive self-organization, fitting along the circumference and demonstrating some elasticity with a slight rotation along the vertical axis. With each pulsation, bubble nucleation sites are observed to shift slightly along the circumference, leading to a slow rotational movement of the patterns. For instance, in a 10 cm deep bed, patterned flows tend to propagate in clockwise rotation, as depicted in Fig. 6a. This type of rotation is not observed in quasi-2D rectangular beds due to the constraints presented by the lateral walls. By unwrapping the domain and positioning the relative bubble centroids in a Lagrangian frame, a hexagonal pattern is revealed that mirrors the one witnessed in a rectangular bed [23], as shown in Fig. 6b.

When applying the same pulsed flow conditions, bubble flows in the annular bed appear slightly less structured as compared to those in quasi-2D rectangular systems. Fig. 7 compares operational windows for rectangular and annular systems, which are characterized by applying the aforementioned model-based pattern recognition method. In both cases, the flows become mainly structured ($\Lambda \geq 0.2$) within a frequency range of 4 - 7 Hz and with sufficiently low amplitudes ($\hat{u}_a = 1.25$ and $\hat{u}_a = 1.75$). In addition, the maximum pattern intensity is also attained under the same flow conditions ($\hat{u}_a = 1.25$, $\hat{u}_{\min} = 0.5$, and $f = 5$ Hz) in a 10 cm deep bed. Similarly, as the amplitude increases, the structures collapse due to the vigorous agitation of the particles [15]. These results show that both systems share similar operational regimes, implying the potential for translating the operational windows to different configurations if particle properties remain consistent.

3.2. Bubble properties in rectangular and annular fluidized beds

The introduction of curved boundary conditions and absence of lateral walls are anticipated to impact the bubble properties and, therefore, alter the emergence of structured flows. As highlighted in our preceding work [23], three major distinctive features can be identified: manipulation of the size of the bubbles, spatial arrangement of the bubbles, and homogenization of bubbling properties. These features arise from the additional flexibility provided by the pulsation and the resulting structuring.

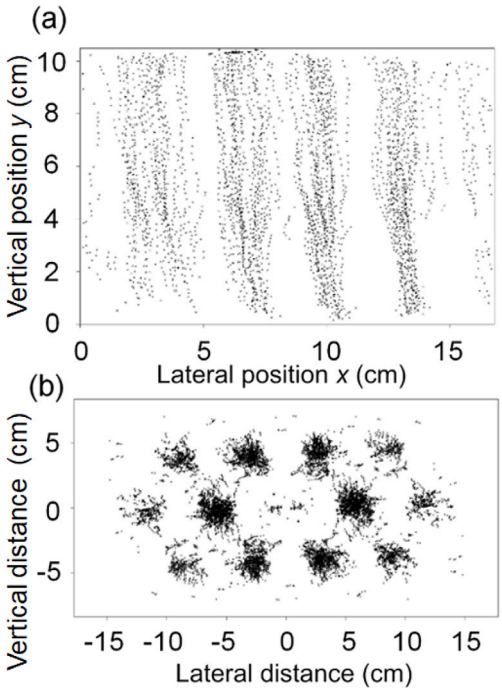

Fig. 6. Bubble arrangement of structured flows within the annular geometry: (a) Absolute bubble positions within the domain, and (b) a Lagrangian frame of the relative bubble positions. The bubbles are sampled from a period of 20 s in the experiment. $d_p = 238$ μm. $\hat{u} = 0.5 + 1.75[1 + \sin(2\pi 5t)]$.

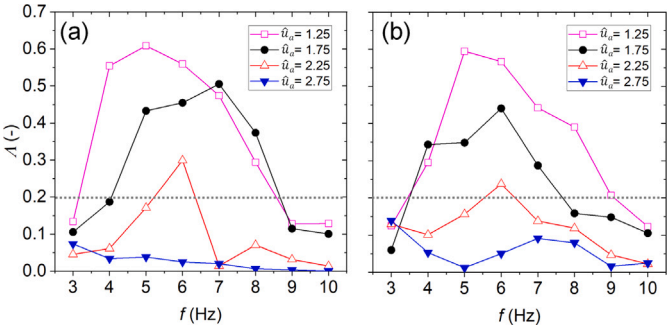

Fig. 7. Pattern intensity, Λ, in 10 cm deep beds in (a) quasi-2D rectangular and (b) annular cylindrical configurations. Flows are considered dynamically structured for $\Lambda \geq 0.2$ (above dotted lines). $f = 3$–10 Hz; $\hat{u}_a = 1.25$–2.75; $\hat{u}_{\min} = 0.5$; $H_b = 10$ cm.

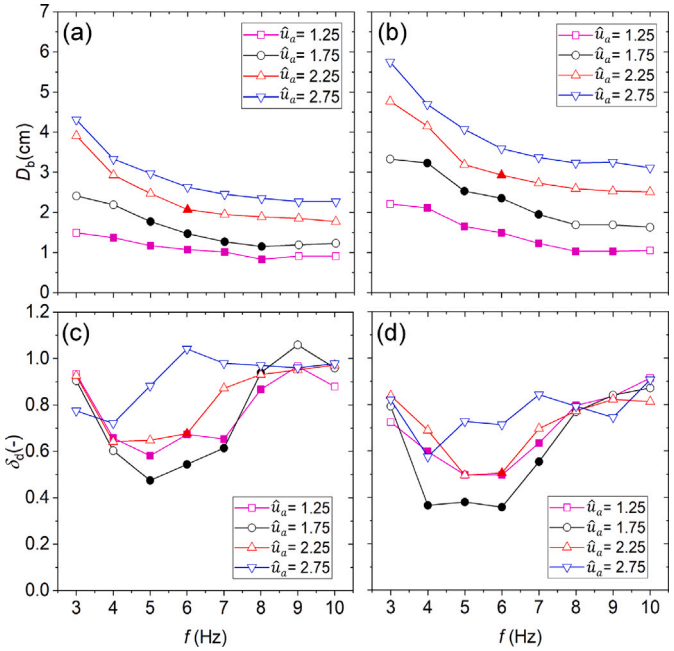

Fig. 8. Influence of pulsation frequency and amplitude on the measured bubble size. (a) Bubble size, D_b, and (c) its span, δ_d, in pulsed quasi-2D rectangular beds; (b) D_b and (d) δ_d in pulsed annular beds. The sizes are computed based on 20 s flow patterns. f = 3–10 Hz; $\hat{u}_a$ = 1.25–2.75; $\hat{u}_{min}$ = 0.5; H_b = 10 cm. Structured ($\Lambda \geq 0.2$) and unstructured flows ($\Lambda < 0.2$) are presented with closed and open symbols, respectively.

3.2.1. Bubble size

Manipulation of bubble size is not exclusively associated with structuring, but is a general characteristic of pulsed beds. By solely altering the frequency, the time-averaged gas velocity remains the same, but the bubble flows can be influenced. Fig. 8 illustrates the change in bubble size in response to adjustments in pulse frequency f and amplitude $\hat{u}_a$. Despite variations in size, the bubbles measured in both configurations display a similar monotonically decreasing trend, reflecting a comparable degree of tunability. As the amplitude increases, bubble size also increases due to the corresponding increase in superficial gas velocity. Specifically, for each designated amplitude, the bubble size D_b dramatically decreases as pulse frequency increases from 3 Hz to 7 Hz, where the flows become structured with less space between bubbles (see representative frames in Fig. 9). The bubble size plateaus at frequencies exceeding 8 Hz, as the particulate bed cannot rapidly respond to the imposed oscillation, resulting in a flow that resembles that observed in a bed with a constant flow. The inability to respond to pulsation leads to bubble coalescence at these high frequencies [33].

The curved boundary barely disrupts the pattern formation, but it modifies the bubble size. By comparing Fig. 8a and b, it can be observed that, under the same flow conditions, bubbles in the annular bed are at least 20% larger in size than in the rectangular bed. Our preliminary tests demonstrated that such an increase in bubble size is also observed in conventional annular beds. Such size difference shows a more efficient gas usage for bubble creation in the annular system compared to the rectangular one. Consequently, the particulate phase in annular beds experiences a higher level of agitation and dilation by the bubbles, which could account for the lower pattern intensity detected (Fig. 7).

3.2.2. Pattern wavelength

The capability to control the spatial arrangement of patterns remains effective when transitioning flow patterns from a rectangular to an annular cylindrical geometry. Despite the constraints imposed on the wavelength, it is remarkable that the pattern manages to adapt along the circumference. This highlights that pattern formation in pulsed fluidized beds is a strongly nonlinear phenomenon. The regular pattern is not a simple standing wave between side walls, which are present in the rectangular setup and absent in the cylindrical annular one. As per the pattern intensity in Fig. 8, a noticeable increase in the measured wavelength occurs between f = 4 Hz and f = 5 Hz, as shown in Fig. 10a, aligning with the transition from an unstructured to a structured state. The wavelength peaks at f = 4 Hz and subsequently reduces monotonically with the applied frequency within the structured regime, specifically between 4 Hz ≤ f ≤ 8 Hz. In order to accommodate the patterns, the wavelength in the annular bed is stretched and the pattern rearranges in the annular bed system, showing a 20% increase in separation under the same flow conditions. With curved front and rear walls, the separation of bubbles is more sensitive to pulse frequency, and λ decreases more obviously with an increase in f.

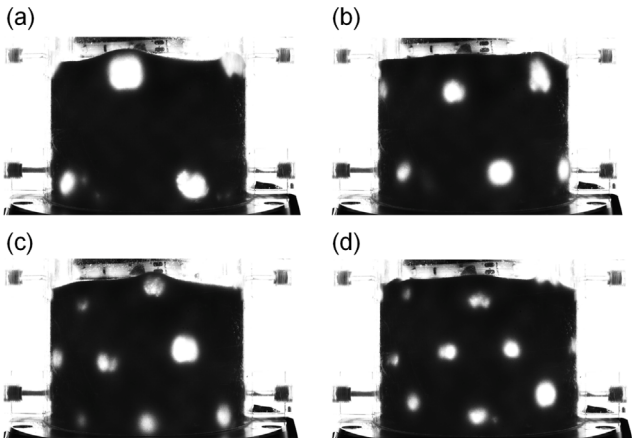

Fig. 9. Representative frames of structured patterns in annular beds with increasing pulsation frequency, f = (a) 4 Hz, (b) 5 Hz, (c) 6 Hz, (d) 7 Hz; $\hat{u}_a$ = 1.25; $\hat{u}_{min}$ = 0.5; H_b = 10 cm. See the Supplementary Material for a video of the flow patterns.

Fig. 10c and d display the variability in bubble separation, measured by δ_λ. As expected, the least variability δ_λ is detected at f = 4 Hz and f = 5 Hz, respectively, aligning with the maximum detected intensities shown in Fig. 7. Within the range of frequencies where patterns appear, minor increases in the wavelengths are observed with increasing amplitude, but the flow patterns degrade significantly into unstructured flows. As demonstrated in our previous work, the persistence of the patterns necessitates flows in between bubbles with a dense particulate phase [15]. The variability of bubble separation in annular beds is generally less than in rectangular beds, showing elasticity and reduced limitations by eliminating the lateral walls.

3.2.3. Homogeneity of bubbling properties

The implementation of a structured flow brings the advantage of more uniform bubbling properties. Bubbles in a highly structured pattern ascend without much mutual interference. The span of the bubble size, δ_d, or separation distribution, δ_λ, serves as a benchmark for quantifying the extent of homogeneity. Fig. 11 showcases plots of δ_d and δ_λ as functions of pattern intensity, Λ, in both pulsed (PB) and conventional fluidized beds (CB). Although there is some scatter, δ_d and δ_λ are observed to be roughly proportional to Λ. As the degree of structuring progressively increases, the spans decrease, showing that the bubbles become increasingly uniform in their characteristics, as evidenced by a narrowing distribution. Bubbles in both quasi-2D rectangular and annular configurations exhibit quantitatively similar correlations of span and intensity, as shown in Fig. 11a–d. This similarity suggests that the feature of increased homogeneity, a key characteristic of structured flows, is effectively retained when transitioning to an annular geometry.

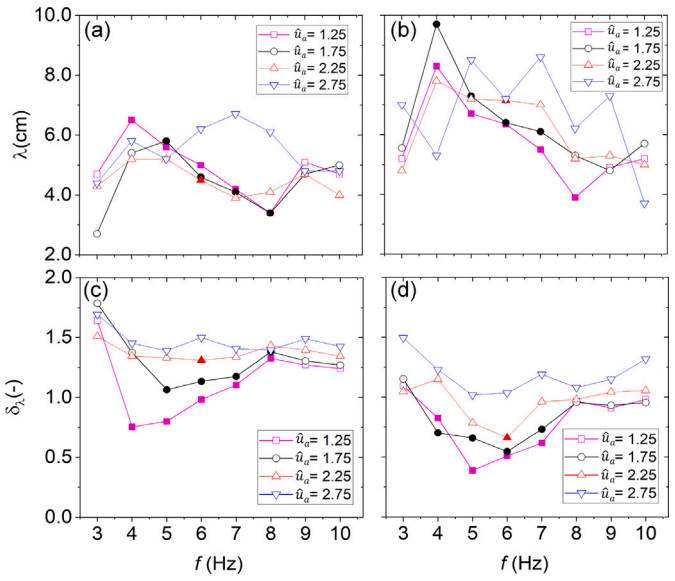

Fig. 10. Influence of pulsation frequency and amplitude on the measured bubble separation. (a) Bubble separation and (c) its span in pulsed rectangular beds; (b) bubble separation and (d) its span in pulsed annular beds. The sizes are computed based on 20 s flow patterns. f = 3–10 Hz; $\hat{u}_a$ = 1.25–2.75; $\hat{u}_{\min}$ = 0.5; H_b = 10 cm. Structured ($\Lambda \geq 0.2$) and unstructured flows ($\Lambda < 0.2$) are presented with closed and open symbols, respectively.

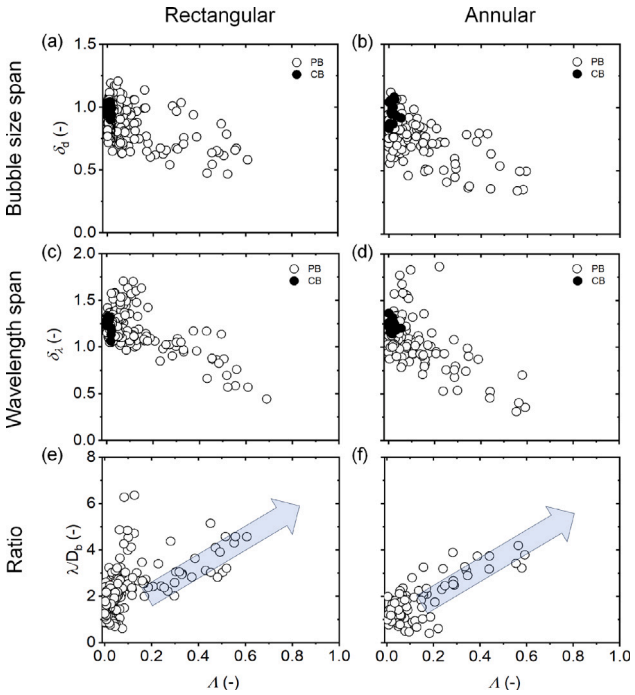

Fig. 11. Correlations between pattern intensity Λ and homogeneity of bubbling size δ_b and separation δ_λ under varying oscillatory flows. (a)–(b) Span of bubble size, (c)–(d) span of bubble separation δ_λ, and (e)–(f) ratio of wavelength-to-bubble diameter, λ/D_b measured in rectangular and annular configurations. The close symbols and open symbols stand for the measurements in fluidized beds at constant flows (CB), and in pulsed beds (PB), respectively. f = 3–10 Hz; $\hat{u}_a$ = 1.25–2.75; $\hat{u}_{\min}$ = 0.5–1.25; H_b = 10 cm.

Additionally, maintaining a relatively large λ/D_b ratio corresponds to a highly structured flow. For instance, Fig. 11e and f show that structured flows of $\Lambda \geq 0.2$ require a λ/D_b greater than 2, in order to prevent bubbles from interfering, and maintain smooth propagation. It is noteworthy that the extensive scatter for $\Lambda \approx 0.1$ and large λ/D_b ratios in Fig. 11e can be attributed to the frequent coalescence of bubbles created at large pulsation frequencies. As the flow becomes more structured, a higher λ/D_b ratio is, therefore, expected. For structured flows of $\Lambda \geq 0.2$, the scattering aligns to reveal a weakly linear trend, and the slope remains consistent across both systems. A correlation can be drawn between these two dimensionless parameters to estimate the suitable conditions to create desired structured flow characteristics:

$$\frac{\lambda}{D_b} \approx 5\Lambda + 1 \tag{5}$$

The experiments suggest consistent criteria for pattern stabilization, irrespective of bed configuration. The commonality between quasi-2D rectangular and annular systems points out the role of achieving an appropriate balance between pattern wavelength and bubble size in developing and maintaining structured flow properties. It should be noted that the slope in the proposed rudimentary, linear correlation depends on the bed depth and particle properties. More elaborate correlations could account for this, based on more extensive studies.

3.3. Simulation of structured flows in the quasi-2D rectangular and annular beds

Our recent work [7] has demonstrated that the CFD-DEM model could successfully capture the experimental alternating bubble flows and provide an accurate prediction of the flow field. Fig. 12 shows the temporal evolution of simulated bubble patterns created at f = 5 Hz in both rectangular and annular configurations. The stages of bubble nucleation, propagation, and rupture are represented with the maps of bubbling probability density f_{b,ϕ_0}. During the rupture stage, for both configurations, bubbles rise and reach the surface, with horizontal positions half a pattern wavelength apart in consecutive pulses (see phase angle $\varphi = 0.2\pi$ and $\varphi = 2.2\pi$). The most significant difference between the rectangular and annular configurations is the rupture stage. For the rectangular configuration, the nucleation stage starts with the formation of a clear horizontal channel above the distributor at $\varphi = 0.6\pi$ when the gas velocity u decreases, and it ends at $\varphi = 1.3\pi$ when u drops below u_{mf}. While for the annular configuration, incipient voids are nucleated at $\varphi = 0.7\pi$ and evolve into inverted conical voids around $\varphi = 1.0\pi$. As these inverted conical voids disconnect from each other and shape into newborn bubbles, they quickly recover rounded shapes and ascend towards the bed surface. This process is denoted as the propagation stage.

This discrepancy is also reflected in the evolution of bubble size and wavelength in the nucleation-propagation-rupture cycle. Fig. 13a exhibits substantial variation in the bubble size during the nucleation stage. During the propagation stage, the bubbles primarily adjust their shape, with only minor variations in size. In the annular configuration, the formation of channel-like slugs is suppressed, which is likely due to the curved boundaries, resulting in an earlier commencement of the propagation stage. As a result, the bubble size in the annular bed is observed to be 20% larger than that in a quasi-2D rectangular bed during the propagation stage. This concurs qualitatively with experimental observations (see Fig. 8). However, due to the limitations of the setup, a direct comparison between the experimental and the simulated flow pattern is not feasible in the 4.5 cm deep annular bed. Specifically, the visualization of experimental bubbles near the distributor is obstructed by the flange.

The pattern wavelength λ remains consistent in both simulated configurations, as depicted in Fig. 13b. Moreover, from $\varphi = 1.6\pi$, the point at which bubbles complete their shape adjustments, the variation in λ stays below 5%, showing that the created pattern is highly reproducible and predictable.

The emergence of locked dense regions of solids between and behind a singular array of ascending bubbles in the rectangular bed is also reproduced in the annular bed, indicated by the marked red

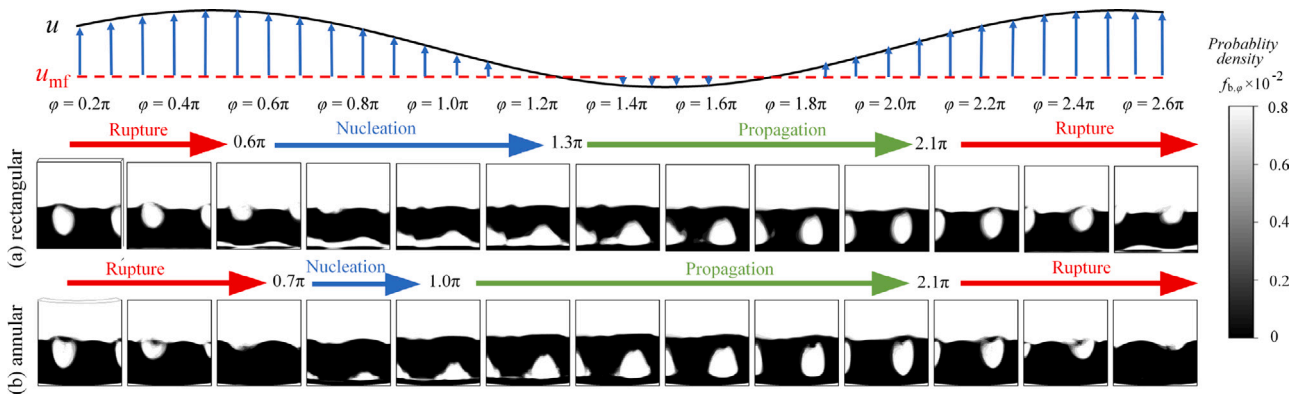

Fig. 12. Maps of bubbling probability density f_{b,ϕ_0} distribution obtained by CFD-DEM simulations in (a) rectangular and (b) annular beds of glass particles, for phase angle φ ranging from 0.2π to 2.6π. Dark, continuous phase represents emulsion phase, whereas bright, dispersed phase stands for gas bubbles. f = 5 Hz; $\hat{u}_a$ = 1.9; $\hat{u}_{\text{min}}$ = 0.45; H_b = 4.5 cm. See the Supplementary Material for a video of the flow patterns.

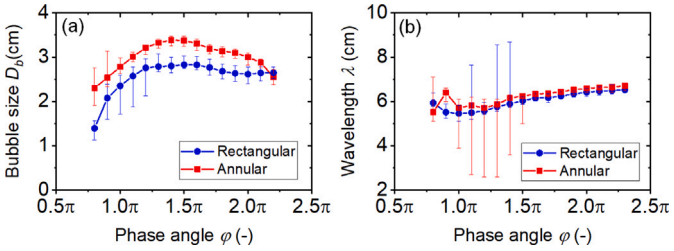

Fig. 13. Time evolution of (a) bubble size D_b and (b) wavelength λ in fluidized beds pulsed at 5 Hz. Bubble size and wavelength are presented as a function of the gas flow phase angle for annular cylindrical and rectangular fluidized bed simulations. The data are obtained over 7 s (in total 35 pulse periods). The error bars between the top and bottom of each point stand for 90% (D90) and 10% (D10) of the measured distribution. f = 5 Hz; $\hat{u}_a$ = 1.9; $\hat{u}_{\text{min}}$ = 0.45; H_b = 4.5 cm.

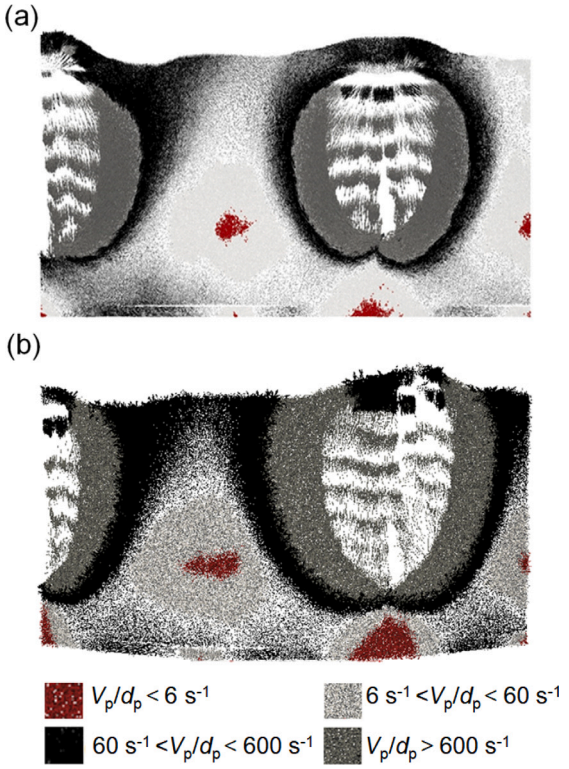

Fig. 14. Illustration of the dense areas of structured flows in (a) quasi-2D rectangular and (b) annular cylindrical beds at $\varphi = 2\pi$. V_p is the particle velocity obtained from DEM, red: $\frac{V_p}{d_p} < 6\ \text{s}^{-1}$; light-gray: $6\ \text{s}^{-1} < \frac{V_p}{d_p} < 60\ \text{s}^{-1}$; black: $60\ \text{s}^{-1} < \frac{V_p}{d_p} < 600\ \text{s}^{-1}$; dark-gray: $\frac{V_p}{d_p} > 600\ \text{s}^{-1}$. f = 5 Hz; $\hat{u}_a$ = 1.9; $\hat{u}_{\text{min}}$ = 0.45; H_b = 4.5 cm.

and light gray areas in Fig. 14. Most of the gas introduced through the distributor immediately diverges to bypass the locked, dense regions, while employing the ascending bubbles as shortcuts to travel towards the top surface. Both the annular and rectangular beds feature locked regions of similar area, even though those in the annular configuration display reduced mobility, characterized by lower particle velocities (represented by the increased red area). This phenomenon is associated with the observed depression of the channel-like structure by the curved boundary, which is more effective in redirecting the gas flow. Consequently, the increased locked regions between the bubbles cause more distinct compartmentalization within the domain.

The alternating nucleation of bubbles leads to periodic switching of the lateral motion of solids, leading to local recirculation. As displayed in Fig. 15a and b, particles in both configurations circulate following an almost identical pattern. The phase-averaged solid velocity profiles in the vicinity of the distributor plate demonstrate that, when the next pulsation period initiates at $\varphi = 2\pi$, particles are only dragged upwards at the locations of bubble nucleation, and travel vertically at speeds of similar magnitudes, as illustrated in Fig. 15c. The solid lateral velocity profiles, captured at $\varphi = 2\pi$ and $\varphi = 0$ (or 4π), appear symmetrical as presented in Fig. 15d, revealing that the solids periodically reverse their direction of travel. It is noteworthy that turning points – where the direction of solid lateral movement changes – occur at the bottom vertex of the bubbles, and the number of these turning points is determined by the number of bubble streams created in the system.

When forming such a structured system, the same compartmentalization characterized by the controlled gas-solid contact time and local solid mixing is preserved, as shown by Vandewalle et al. [17]. As a consequence, the heat and mass transport rates should fall somewhere between those observed in fixed and vigorously fluidized beds. The presence of locked regions inhibits long-range solid recirculation, turning solid mixing in dynamically structured fluidized beds into a localized process, intrinsically associated with columns of rising bubbles. Consequently, the entire domain is partitioned into various compartments, distinguished by two characteristic length scales: bubble size and pattern wavelength. When confining the structured flows within curved boundaries, the pattern formation mechanism is preserved with only minor alterations to the bubble properties. Apart from pulsation conditions, it is to be expected that design parameters, such as bed height and curvature, could influence the bubble properties and the degree of regularity of the structured flows. A deeper bed allows for increased opportunities for bubble interactions, necessitating

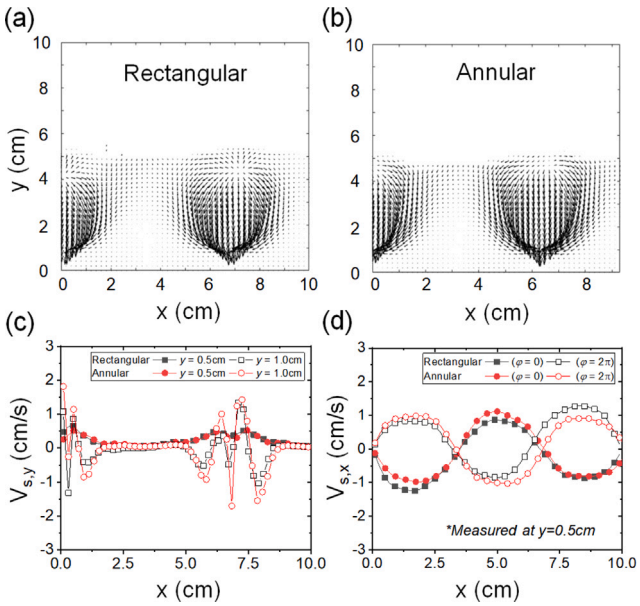

Fig. 15. Solid circulation patterns in the (a) rectangular and (b) annular beds at $\varphi = 2\pi$; (c) Profiles of phase-averaged solids axial velocity $V_{s,y}$ at vertical positions $y = 0.5$ cm and $y = 1.0$ cm for CFD-DEM simulations at $\varphi = 2\pi$, and (d) Profiles of phase-averaged solids lateral velocity $V_{s,x}$ at $y = 0.5$ cm at $\varphi = 2\pi$ and $\varphi = 0$. $f = 5$ Hz; $\hat{u}_a = 1.9$; $\hat{u}_{\min} = 0.45$; $H_b = 4.5$ cm.

modifications to the operating conditions to achieve regular patterns. Furthermore, there is, presumably, a specific minimal annulus diameter essential for achieving structured patterns. A rigorous analysis, considering various design parameters, is essential to further understand and reproduce structured flows within annular beds, and to advance towards practical applications.

4. Conclusions

The flow structure observed in a flat, rectangular fluidized bed is successfully reproduced in an annular system. The absence of lateral walls introduces some disturbances, yet the structured pattern of bubbles is remarkably preserved. In addition, the mechanism and the criteria for forming structured flows remain consistent for wall-bounded beds. However, for an annular bed, applying the same flow conditions leads to larger bubbles and a rising, periodic bubble pattern that fits along the bed's circumference. Our study demonstrates that the unique features of structured flow, such as control over bubble size and separation distribution, are successfully translated and preserved in more complex geometries. These characteristics should be highly beneficial in practical applications, as they allow to avoid some challenges in conventional fluidized bed units, like flow maldistribution and non-uniform contact, as well as decouple conflicting design objectives, such as efficient solid mixing and gas-solid contact.

Further scaling up this phenomenon to an industrial scale would represent a step-change solution to design gas-solid processes, from drying to coating and multiphase reactions. It could facilitate process intensification, and reduce capital requirements. The feasibility of extending the structured flows to different geometries has been proven using lab-scale flat and annular units. A more comprehensive analysis remains necessary to quantitatively address the effects of design parameters, such as curvature, bed height, and boundary conditions, on the regularity and stability of structured flows, in order to facilitate further scale-up. Further demonstration of mass and heat transfer properties, robustness and reproducibility under industrially relevant conditions will provide a major advance towards commercialization.

CRediT authorship contribution statement

Kaiqiao Wu: Data curation, Formal analysis, Investigation, Software, Visualization, Writing – original draft. **Shuxian Jiang:** Data curation, Formal analysis, Investigation, Software, Validation, Visualization, Writing – original draft. **Victor Francia:** Methodology, Supervision, Writing – review & editing. **Marc-Olivier Coppens:** Conceptualization, Funding acquisition, Methodology, Project administration, Supervision, Writing – review & editing.

Declaration of competing interest

The authors declare that they have no known competing financial interests or personal relationships that could have appeared to influence the work reported in this paper.

Data availability

Data will be made available on request.

Acknowledgments

The research leading to these results has received funding from an EPSRC, United Kingdom "Frontier Engineering" Award (EP/K038656/1, EP/S03305X/1) as well as a PhD scholarship from Synfuels China Co., Ltd.

Appendix A. Supplementary data

Supplementary material related to this article can be found online at https://doi.org/10.1016/j.powtec.2023.119096.

References

[1] D. Kunii, O. Levenspiel, Fluidization Engineering, second ed., Butterworth-Heinemann, Boston, 2013, http://dx.doi.org/10.1016/C2009-0-24190-0.
[2] J.R. Grace, Hydrodynamics of bubbling fluidization, in: Essentials of Fluidization Technology, John Wiley & Sons, Ltd, 2020, pp. 131–152, http://dx.doi.org/10.1002/9783527699483.ch7.
[3] M.-O. Coppens, J.R. van Ommen, Structuring chaotic fluidized beds, Chem. Eng. J. 96 (2003) 117–124, http://dx.doi.org/10.1016/j.cej.2003.08.007.
[4] M. Rüdisüli, T.J. Schildhauer, S.M.A. Biollaz, J.R. van Ommen, Scale-up of bubbling fluidized bed reactors — A review, Powder Technol. 217 (2012) 21–38, http://dx.doi.org/10.1016/j.powtec.2011.10.004.
[5] L.R. Glicksman, M. Hyre, K. Woloshun, Simplified scaling relationships for fluidized beds, Powder Technol. 77 (1993) 177–199, http://dx.doi.org/10.1016/0032-5910(93)80055-F.
[6] M. Horio, A. Nonaka, Y. Sawa, I. Muchi, A new similarity rule for fluidized bed scale-up, AIChE J. 32 (1986) 1466–1482, http://dx.doi.org/10.1002/aic.690320908.
[7] V. Francia, K. Wu, M.-O. Coppens, Dynamically structured fluidization: oscillating the gas flow and other opportunities to intensify gas-solid fluidized bed operation, Chem. Eng. Process. Process Intensif. 159 (2021) 108143, http://dx.doi.org/10.1016/j.cep.2020.108143.
[8] S. Maurer, E.C. Wagner, J.R. van Ommen, T.J. Schildhauer, S.L. Teske, S.M.A. Biollaz, A. Wokaun, R.F. Mudde, Influence of vertical internals on a bubbling fluidized bed characterized by X-ray tomography, Int. J. Multiph. Flow 75 (2015) 237–249, http://dx.doi.org/10.1016/j.ijmultiphaseflow.2015.06.001.
[9] J.M. Valverde, M.J. Espin, M.A.S. Quintanilla, A. Castellanos, Fluid to solid transition in magnetofluidized beds of fine powders, J. Appl. Phys. 108 (2010) 054903, http://dx.doi.org/10.1063/1.3480989.
[10] F. Raganati, R. Chirone, P. Ammendola, Calcium-looping for thermochemical energy storage in concentrating solar power applications: Evaluation of the effect of acoustic perturbation on the fluidized bed carbonation, Chem. Eng. J. 392 (2020) 123658, http://dx.doi.org/10.1016/j.cej.2019.123658.
[11] D. Jia, O. Cathary, J. Peng, X. Bi, C.J. Lim, S. Sokhansanj, Y. Liu, R. Wang, A. Tsutsumi, Fluidization and drying of biomass particles in a vibrating fluidized bed with pulsed gas flow, Fuel Process. Technol. 138 (2015) 471–482, http://dx.doi.org/10.1016/j.fuproc.2015.06.023.
[12] K. Wu, E.C. Wagner, O. Ochkin-Koenig, M. Franck, D. Weis, G.M.H. Meesters, J.R. van Ommen, Time-resolved X-ray study of assisted fluidization of cohesive micron powder: On the role of mechanical vibration, Chem. Eng. J. 470 (2023) 143936, http://dx.doi.org/10.1016/j.cej.2023.143936.

[13] D. Jia, X. Bi, C.J. Lim, S. Sokhansanj, A. Tsutsumi, Gas-solid mixing and mass transfer in a tapered fluidized bed of biomass with pulsed gas flow, Powder Technol. 316 (2017) 373–387, http://dx.doi.org/10.1016/j.powtec.2016.10.031.
[14] H. Li, L. Wang, T. Wang, C. Du, Experimental and CFD-DEM numerical evaluation of flow and heat transfer characteristics in mixed pulsed fluidized beds, Adv. Powder Technol. 31 (2020) 3144–3157, http://dx.doi.org/10.1016/j.apt.2020.06.004.
[15] K. Wu, L. de Martín, M.-O. Coppens, Pattern formation in pulsed gas-solid fluidized beds: the role of granular solid mechanics, Chem. Eng. J. 329 (2017) 4–14, http://dx.doi.org/10.1016/j.cej.2017.05.152.
[16] Y. Cheng, S. Kaart, M.-O. Coppens, C.M. van den Bleek, Control of chaotic dynamics in a 2D fluidized bed by periodic gas injection, in: Proc. of AIChE Annual Meeting, Vol. 31, 1999, pp. 312–319.
[17] L.A. Vandewalle, V. Francia, K.M. Van Geem, G.B. Marin, M.-O. Coppens, Solids lateral mixing and compartmentalization in dynamically structured gas–solid fluidized beds, Chem. Eng. J. 430 (2022) 133063, http://dx.doi.org/10.1016/j.cej.2021.133063.
[18] M.-O. Coppens, M.A. Regelink, C.M. van den Bleek, Pulsation induced transition from chaos to periodically ordered patterns in fluidised beds, in: Proc. of 4th World Congr. on Part. Technol. (WCPT4), Vol. 355, 2002, pp. 1–8.
[19] F. Melo, P.B. Umbanhowar, H.L. Swinney, Hexagons, kinks, and disorder in oscillated granular layers, Phys. Rev. Lett. 75 (1995) 3838, http://dx.doi.org/10.1103/PhysRevLett.75.3838.
[20] M. Saidi, H. Basirat Tabrizi, J.R. Grace, C.J. Lim, G. Ahmadi, Hydrodynamic and mixing characteristics of gas–solid flow in a pulsed spouted bed, Ind. Eng. Chem. Res. 54 (2015) 7933–7941, http://dx.doi.org/10.1021/acs.iecr.5b01645.
[21] D.V. Pence, D.E. Beasley, Chaos suppression in gas-solid fluidization, Chaos 8 (1998) 514–519, http://dx.doi.org/10.1063/1.166332.
[22] L. de Martín, C. Ottevanger, J.R. van Ommen, M.-O. Coppens, Universal stability curve for pattern formation in pulsed gas-solid fluidized beds of sandlike particles, Phys. Rev. Fluids 3 (2018) 034303, http://dx.doi.org/10.1103/PhysRevFluids.3.034303.
[23] K. Wu, Dynamically Structured Flow in Pulsed Fluidised Beds, Springer Nature, Cham, 2021, http://dx.doi.org/10.1007/978-3-030-68752-6.
[24] Q. Guo, Y. Zhang, A. Padash, K. Xi, T.M. Kovar, C.M. Boyce, Dynamically structured bubbling in vibrated gas-fluidized granular materials, Proc. Natl. Acad. Sci. 118 (2021) e2108647118, http://dx.doi.org/10.1073/pnas.2108647118.
[25] Q. Guo, C.M. Boyce, Structured bubbling in layered gas-fluidized beds subject to vibration: A CFD-DEM study, AIChE J. 68 (2022) e17709, http://dx.doi.org/10.1002/aic.17709.
[26] T. Li, J.R. Grace, X. Bi, Study of wall boundary condition in numerical simulations of bubbling fluidized beds, Powder Technol. 203 (2010) 447–457, http://dx.doi.org/10.1016/j.powtec.2010.06.005.
[27] A. Bakshi, Multiscale Continuum Simulations of Fluidization: Bubbles, Mixing Dynamics and Reactor Scaling (Ph.D. thesis), Massachusetts Institute of Technology, 2017.
[28] J.E. Higham, M. Shahnam, A. Vaidheeswaran, Anomalous diffusion in a bench-scale pulsed fluidized bed, Phys. Rev. E 103 (2021) 043103, http://dx.doi.org/10.1103/PhysRevE.103.043103.
[29] C. Goniva, C. Kloss, N.G. Deen, J.A.M. Kuipers, S. Pirker, Influence of rolling friction on single spout fluidized bed simulation, Particuology 10 (2012) 582–591, http://dx.doi.org/10.1016/j.partic.2012.05.002.
[30] D. Gidaspow, Multiphase Flow and Fluidization: Continuum and Kinetic Theory Descriptions, Academic Press, New York, 1994, http://dx.doi.org/10.1016/C2009-0-21244-X.
[31] C. Wen, Y. Yu, Mechanics of fluidization, Chem. Eng. Prog. Symp. Ser. 62 (2013) 100.
[32] S. Ergun, Fluid flow through packed columns, Chem. Eng. Prog. 48 (1952) 89–94.
[33] M. Saidi, H. Basirat Tabrizi, J.R. Grace, A review on pulsed flow in gas-solid fluidized beds and spouted beds: Recent work and future outlook, Adv. Powder Technol. 30 (2019) 1121–1130, http://dx.doi.org/10.1016/j.apt.2019.03.015.